[SLAC-PUB-9341]
March 2002

Morphology of Thermoplastic Elastomers: Stereoblock Polypropylene [*] [§]

Holger Schönherr, Willy Wiyatno, Curtis W. Frank, Gerald G. Fuller, Alice P. Gast
Department of Chemical Engineering, Stanford University, Stanford CA 94305-5025

John A. Pople
Stanford Synchrotron Radiation Laboratory, Stanford Linear Accelerator Center, Stanford University, Stanford, CA 94309

Robert M. Waymouth
Department of Chemistry, Stanford University, Stanford CA 94305-5080

Abstract

The morphologies of low-density (0.86 g/cm^3), elastomeric polypropylene (ePP) derived from bis(2-arylindenyl) hafnium dichloride were investigated using a combination of polarized optical microscopy (OM), differential scanning calorimetry (DSC), wide angle X-ray scattering (WAXS), Fourier transform infrared (FT-IR) spectroscopy, and tapping mode atomic force microscopy (TM-AFM). These low-crystallinity polypropylenes, when crystallized isothermally from the melt, exhibit morphologies reminiscent of classical semi-crystalline polymers. The presence of lamellae, cross-hatching, hedrites, and spherulites was revealed by high resolution TM-AFM. These elastomeric polypropylenes can be fractionated into components of different average tacticities and crystallinities, but similar molecular mass. The analysis of the morphologies of all of the fractions revealed both large hierarchical structures and cross-hatching typical of the α-modification of crystalline isotactic polypropylene for all but the lowest crystalline ether soluble fraction. Evidence for high-melting crystals in all of the fractions are most consistent with a stereoblock microstructure of atactic and isotactic sequences.

Keywords

atomic-force microscopy; group-ivb catalysts; isotactic polypropylene; zirconocene catalysts; poly(ethylene oxide); lamellar morphology; polymer structure; crystallization; poly(propylene); spherulites

Submitted to Macromolecules

[*] Work supported by Department of Energy contract DE-AC03-76SF00515
[§] Work supported by NSF Center on Polymer Interfaces and Macromolecular Assemblies (CPIMA)

Introduction

Many recent developments in polymer materials science have been triggered by the development of improved synthetic methods, including the development of single site catalysts for controlled polymerizations,[1,2,3] novel polymerization techniques,[4,5] and highly specific polymerizations using cloning strategies.[6] As a consequence, a wide variety of polymers with unusual properties can be designed and synthesized. New synthetic techniques are providing higher levels of control over composition, molecular mass distributions, branching, and stereoregularity.[1] For instance, thermoplastic elastomers based on polypropylene have been known since the 50's.[7] New catalysts and synthetic strategies have led to new classes of these materials and fresh insights into the origin of their elastomeric properties.[8,9,10] The structure and properties of elastomeric polypropylenes derived from bis(2-arylindene) metallocenes[10] have been the subject of study by a variety of techniques.[11,12] These materials exhibit properties that are both similar to and in some cases distinct from those prepared by other synthetic methods.[11]

The elastomeric polypropylenes (ePP) are characterized by a low, but still significant degree of crystallinity.[11,12] The crystalline domains of these low-crystallinity polypropylenes are thought to serve as physical crosslinks.[7] The size and distribution of these crystalline regions in the amorphous matrix should have an important influence on the mechanical properties of these thermoplastic elastomers. It is therefore of particular interest to analyze and understand (1) how, and to what extent, these polyolefin elastomers crystallize and (2), how the materials' properties are related to and possibly determined by the underlying semi-crystalline morphology.

As previously reported, elastomeric polypropylenes derived from 2-arylindene metallocenes can be fractionated into different fractions. These fractions differ in tacticity and crystallinity, but do not differ strongly in molar mass.[11] This feature enables one to study crystallinity, as well as mechanical properties, as a function of stereoregularity. To date, the crystallinity of these materials has been investigated by DSC and x-ray diffraction.[11] The low crystallinity of ePP of (ca. 10%) is a consequence of the low isotacticity (pentad analysis [mmmm]) of 34% as determined by ^{13}C NMR. In contrast, the crystallinity of a typical highly isotactic polypropylene is on the order of 60%, depending on the thermal history. Previous attempts to characterize the underlying morphology of ePP and its lower molar mass fractions in transmission electron microscopy investigations have been inconclusive.

Kravchenko and coworkers were recently successful in imaging the morphology of ePP and the changes in surface morphology resulting from tensile extension experiments by tapping-mode atomic force microscopy (TM-AFM).[12] Based on TM-AFM images these authors showed that the unstrained ePP crystallizes in the form of individual, short lamellae embedded in an amorphous matrix. This morphology is markedly different from the morphology found for isotactic polypropylene (iPP) and was attributed to the much lower crystallinity of the elastomeric polypropylene. The α and β-modifications of iPP,[13] both of which have been extensively studied by scanning probe microscopic approaches,[14,15,16] are well-understood from the micrometer to the nanometer level.[17]

In this contribution, we show that polypropylenes with densities as low as 0.86 g/cm^3 can be crystallized isothermally to yield crystalline morphologies of higher order, including lamellae and cross-hatched lamellae, which can organize into hedrites or spherulites, depending on the overall crystallinity as well as thermal history.

Experimental

Materials. The elastomeric polypropylene (ePP) was synthesized by BP Amoco Chemical Company (PP-22010) in liquid propylene at 50^{o}C using bis(2-(3,5-di-t-butylphenyl)indenyl) hafnium dichloride as catalyst.[18] Fractionation was carried out by successive solvent extraction of ePP with boiling diethyl ether and heptane under a nitrogen environment following the procedure reported previously.[11] Three fractions with an increasing isotacticity were obtained: ether soluble (ES, lowest isotacticity), heptane soluble (HS, medium isotacticity), and heptane insoluble (HI, highest isotacticity) (see Table 1). A blend material was obtained by blending the lowest isotacticity (ES) and the highest isotacticity (HI) fractions to match the average isotacticity ([mmmm]) of the parent ePP sample. Blending was carried out by dissolving the fractions in boiling xylene followed by precipitation into an excess of methanol and drying in vacuo. Table 1 shows the characterization data of the elastomeric polypropylene ePP together with its fractions.[18]

Sample preparation. All the samples investigated were initially melt-pressed between two protective Teflon sheets (Mechanical Grade PTFE, McMaster-CARR) at 180°C under a pressure of 2500 psi in a hot-press (model C, Carver, Menomonee Falls, WI). The film samples

obtained had a typical thickness of ca. 0.5 mm. Subsequently, samples were melted at 180°C in a custom built hot-stage (based on a model PC-600, Corning, Acton, MA) equipped with a temperature controller (CSS-8094 Omega, Stamford, CT) in an argon atmosphere. After melting, the samples were either cooled down to room temperature with a typical rate of 5°C (non-isothermal crystallization) or they were crystallized isothermally (e.g. at 120°C) for 6 hours and quenched with liquid nitrogen.[19] To ensure a consistent thermal history for both isothermal and non-isothermal crystallization, all samples of a given thermal history were prepared simultaneously.

For the AFM and FT-IR experiments, pressed samples were transferred onto pre-cleaned silicon wafers and melted with uncovered free surfaces at 180°C in argon. A number of thin films of isotactic polypropylene (Aldrich) were imaged as reference samples. The sample shown in Figure 1 was prepared by spincoating a solution of ePP in xylenes at high temperatures onto a pre-cleaned silicon wafer followed by exhaustive drying in vacuo for several days.[20] For the optical microscopy study, samples placed on microscope slides (with cover slides) were melt-pressed to a thickness of around 50 microns before being thermally treated.

Tapping mode AFM (TM-AFM). The TM-AFM data was acquired in ambient with a NanoScope III multimode AFM (Digital Instruments (DI), Santa Barbara, CA) using microfabricated silicon tips / cantilevers (Nanosensors, Wetzlar, Germany).[21] Height (constant amplitude damping), amplitude (error signal), and phase images were recorded simultaneously at multiple locations on at least two specimens.[22] While the height images show the profile of the

sample surface quantitatively (assuming that the oscillation of the cantilever is damped similarly at all locations), the amplitude and phase images emphasize the features imaged (here the contrast depends on various imaging conditions, thus no z-scale is provided in the Figure Captions). In the amplitude images the outlines of topographical features, such as radiating fibrillar structures, are seen. The adjusted setpoint ratio of ca. 0.7 to 0.8 results in a stiffness-dominated contrast in the phase images and allowed us to differentiate between stiff crystalline features (i.e. lamellae) and the less stiff amorphous phase.[23,24] The images shown here were subjected to a first order planefitting procedure to compensate for sample tilt. Using the "bearing analysis" (DI NanoScope software), which is a quantitative analysis of the distribution of depths present in the image, we assessed the crystallinity in a semi-quantitative manner. The estimate was based on the assumption that bright contrast in the TM-AFM phase images corresponds exclusively to the crystalline phase, whereas dark contrast corresponds to the amorphous phase.

Optical microscopy (OM). The optical light microscopy investigations were carried out with an optical microscope (Axioplan D-7082, Zeiss) in transmission mode with crossed polarizers. A digital camera (Hamamatsu C4742-95) connected to a personal computer was used to capture the optical microscopy images.

Differential scanning calorimetry (DSC). Thermal analysis was performed on a Perkin Elmer 7 differential scanning calorimeter using indium as calibration standard. Melt-pressed polymers with a thickness of about 0.1 mm were frozen in liquid N_2 and punched-cut with a standard single-hole paper puncher. Disk-like samples of 5 to 15 mg were weighed and sealed into Perkin

Elmer aluminum DSC pans. The thermal treatment of DSC samples was carried out in the DSC instrument under N_2 atmosphere. All samples were initially pre-heated to 200°C with a rate of 40°C/min and held at 200°C for 5 minutes. For non-isothermal thermal history, samples were cooled from 200°C to room temperature at 20°C/min. The isothermal samples were cooled from 200°C to 120°C at 20°C/min and annealed for 6 hours. After annealing, samples were cooled down to room temperature using the same cooling rate. All samples were aged for at least 20 hours at room temperature. After aging, samples were cooled to –25°C at 20°C/min and held for 5 minutes before endotherm scans were carried out. Melting points (T_c) (peak of endotherm curve) and heat of fusion (ΔH_f) were measured by heating from –25°C to 200°C with a rate of 20°C/min. The crystallinity was calculated by normalizing the heat of fusion (ΔH_f) from the endotherm scans by the theoretical value of a completely crystalline sample of 209 J/g.[25]

Wide angle X-ray scattering (WAXS). WAXS experiments were performed at the Stanford Linear Accelerator Center (SLAC) on beamline 1-4 of the Stanford Synchrotron Radiation Laboratory (SSRL). The X-ray source is focused with a flux ~10^{10} photons and monochromated by a (111) Si crystal to a wavelength of λ =1.488 Å. A CCD-based area detector (Photonic Science) with a 1024x1024 array of 25μm square pixels was used to collect the 2-D diffraction data image. Images were assembled from the summation of 1000 consecutive scans, and the portion of reciprocal space imaged was calibrated with a Lupolen standard. Data analysis was performed using 1-D profiles summed radially from the 2-D patterns and corrected for background scattering and scattering from windows associated with the optics. The scattering

intensities are presented as a function of the scattering vector q, which is defined as $q = [4\pi \sin(\Theta/2)] / \lambda$.

Fourier transform infrared spectroscopy (FT-IR). The FT-IR data were obtained on thin films on a BIO-RAD FTS-60A FT-IR spectrometer operated in transmission mode. 64 to 128 scans were collected with a resolution of 2 cm^{-1} and ratioed against the previously collected background spectrum. The absorbances of the bands at ca. 998 cm^{-1} and ca. 975 cm^{-1} were integrated using the peak fitting procedures of the BIO-RAD WIN-IR Pro software. The ratio of these two bands were previously shown to be nearly linearly dependent on the crystallinity of iPP.[26] The IR index A_{998}/A_{975} provides a measure of isotactic helix content; the band at 998 cm^{-1} corresponds to helical conformation of sequence lengths of approximately 10-14 isotactic repeat units, whereas 975 cm^{-1} band corresponds to head-to-tail sequences of propylene units[27].

Results

The morphology of melt crystallized films of the unfractionated ePP was investigated by tapping-mode atomic force microscopy (TM-AFM). As shown in Figure 1, a 200 nm thin film of unfractionated ePP crystallized at 130°C formed giant two-dimensional spherulites. From this low magnification AFM micrograph, the preferred initial growth direction, the branching and splaying of stacks of lamellae under small angles, the filling of the space in the eyes or so-called Popoff's leaves,[28] and the final attainment of the spherical envelope can be clearly seen. This image

corresponds very well to images obtained by various microscopic techniques on classical semicrystalline polymers and agrees with the established view of how typical polymer spherulites develop by nucleation and growth.[29,30] It should be mentioned that this first example for the presence of crystallization and concomitant hierarchical ordering in isothermally crystallized ePP was obtained in a thin film with a thickness of 200 nm as measured by ellipsometry.[20]

Very similar morphologies can be found at the surface of bulk films of unfractionated ePP. Intermediate stages of development of spherulitic growth, so-called hedrites,[31] are depicted in Figure 2 together with a higher magnification micrograph of regions next to the hedrites, which shows edge-on lamellae and a dense cross-hatching pattern. The observation of the so-called cross-hatched morphology with lamellar branching at crystallographically defined angles in these ePP samples is evidence for the presence of the monoclinic α-modification of iPP.[32] The angles measured for the ePP specimens was 80° ± 2°, which compares favorably with the theoretically predicted / observed angle of 80.4°.[32c] The observation of thick dominant lamellae, branching with a defined angle of 80°, and thin branches agrees well with the results of previous morphological studies on iPP.[28,33] The large scale organization in the non-isothermally crystallized film (Figure 3) is less perfect and the observed features are smaller, however, the presence of clear cross-hatching can be noted as well.

From cross-sectional plots we estimate a convoluted average lamellar thicknesses of 20 nm ± 3 nm, 23 nm ± 4 nm, 28 nm ± 6 nm for ePP crystallized isothermally at 110°C, 120°C, and 130°C, respectively. A quantitative determination of lamellar thicknesses of edge-on lamellae from high-

resolution images must be considered inaccurate due to tip convolution. While these values are likely to be overestimates,[34] they are comparable to lamellar thicknesses reported for iPP in the literature.[35]

Optical microscopy with crossed polarizers was used to complement the AFM technique for the characterization of the morphology of ePP. Figure 4 shows a typical OM image of unfractionated ePP crystallized isothermally at 120^{o}C (left) and crystallized non-isothermally (right). A typical Maltese cross spherulite extinction pattern is not observed due to the limited size and imperfection of the hedrites and spherulites. However, the presence of birefringent circular / elliptical features which radiate from central points is obvious. These OM results indicate that the morphologies which were observed by TM-AFM at the free surface of the samples are representative for the whole film.[36] The non-isothermally crystallized samples show little birefringence and no discernible morphological features, which is consistent with small disordered crystallites seen by TM-AFM. The TM-AFM and OM data clearly show that unfractionated ePP can crystallize to a certain extent. In order to analyze the crystallization behavior in more detail, DCS and WAXS studies of ePP and its fractions were performed. These data will be subsequently compared to the morphology as observed by TM-AFM.

Thermal analysis was carried out for ePP and each fraction with DSC comparing isothermally (120^{o}C for six hours) and non-isothermally crystallized samples (Figure 5). The non-isothermally crystallized ePP shows a broad melting transition with two dominant peaks centered at 42^{o}C and 149^{o}C. Isothermal crystallization results in a shift of the melting peaks to 50^{o}C and 150^{o}C,

respectively, and the appearance of another melting peak at 135°C. For the HS fraction, there was only one dominant peak centered at 42°C, which was shifted to 50°C upon isothermal crystallization. The HI fraction had a broad melting range with the first peak at 47°C extending up to another peak at 155°C. After isothermal crystallization, the lower temperature melting peak was shifted to 57°C and the higher temperature melting peak (shifted to 158°C) became more pronounced with an additional melting shoulder peak at around 142°C. The thermal behavior of the blend sample was similar to the HI fraction. The ES fraction showed only barely measurable endotherms in the DSC thermal analysis (endotherm scan not shown). The crystallinities as determined by DSC and WAXS are summarized in Table 2.

Wide angle x-ray scattering experiments were performed to study the effect of thermal history on the crystallinity. Isothermal crystallization conditions (120°C for 6 hours) were contrasted with non-isothermal crystallization conditions (Figure 6). The crystalline peaks in the 2θ plots of unfractionated ePP, HS, HI, and the blend fractions are reflections of the α-phase of iPP.[13] The lowest isotacticity fraction (ES) shows a typical smectic phase.[11,37] Crystallinity was calculated from the ratio of the area of the corresponding peaks (after subtraction of the amorphous halo) to the total area under the curves. As shown in Table 2, isothermal crystallization results in a minute increase in crystallinity as measured by WAXS. The crystallinity as measured by WAXS for each fraction is in good agreement with the crystallinity measured by DSC.

Isothermal crystallization also affected the structure of the unit cell of the crystals, as can be seen from the 2θ plots in Figure 6. After isothermal crystallization the crystalline peaks were shifted to

higher 2θ values, indicative of a decrease in the unit cell dimensions. This is in agreement with the observation of Cheng et. al on the effect of decreasing supercooling on the unit cell dimensions of isotactic polypropylenes.[38] The shift of the crystalline peaks is larger for the higher 2θ value peaks. The isothermal crystallization also resulted in resolving the two peaks around 20.5^{o} of the single peak in the non-isothermal crystallization samples.

In Figure 7, the crystallinity data as determined by WAXS for the various fractions crystallized at 120°C is summarized together with the values derived from DSC, TM-AFM, and FT-IR spectroscopy data. There is a good qualitative agreement between the results obtained by conventional techniques and the rough estimate of surface crystallinity based on TM-AFM images. These results are further supported by the FT-IR data, which deviate not unexpectedly for the low crystallinity ES fraction due to non-linearities in the ratio of absorbances vs. density curves.[26]

Despite its low crystallinity (8-11% as determined by WAXS and DSC), ePP can crystallize to form large hierarchical morphologies that are reminiscent of classical semi-crystalline polymers. The nature of these morphologies depends both on the tacticity of the polymer and the thermal history, as revealed by investigations of the fractions of ePP. The non-isothermally crystallized ePP specimens also display the hierarchical ordering known from iPP,[14,15,17,28,29,31] including the presence of cross-hatching of α-iPP. In the following paragraphs we will discuss the differences in morphology, as visualized by TM-AFM, of the different fractions of ePP which were obtained by boiling solvent extraction (Table 1). Each fraction shows distinctively different morphological

details, but images of the heptane-soluble and heptane-insoluble fractions reveal morphologies typical for isothermally crystallized films, i.e. lamellae, hedrites, and spherulites.[14,15,17,29,28] In contrast, the low crystallinity ES fraction displays only individual lamellae or "bundles" of lamellae in isothermally crystallized samples. In most cases the lamellae were observed in edge-on orientation. Occasionally we observed individual flat-on lamellae for the ES fraction (vide infra). Crosshatching,[32] which indicates the presence of the α-phase of iPP, is found in the HI and HS fractions, the blend, and the unfractionated ePP (vide supra), but not in the ES fraction. Nevertheless, the morphological features observed by TM-AFM provide good evidence for crystallinity in all fractions, including the lowest-tacticity ES fraction.

Similar morphologies are observed for the HI and HS fractions as shown in Figure 8 and Figure 9, respectively. In general, we can observe spherulites and hedrites in various stages of development. However, the nucleation density and perfection of these aggregates differed significantly for the different fractions. While the HI fraction formed spherulitic entities, the HS fraction formed isolated large hedrites, very similar to the parent ePP. This qualitative difference in morphology may be attributed to a smaller fraction of crystallizable material derived from long stereoregular sequences in the lower crystallinity samples. In addition, the high degree of crystallinity in the HI fraction is reflected in the almost exclusive presence of bright lamellar features in the phase image shown in Figure 8 (right). Non-isothermal crystallization of the HI and HS fractions resulted in much less well defined hedritic or spherulitic features, presumably due to the faster crystallization kinetics at lower temperatures during cooling. However, it should be noted that rather well-developed cross-hatching was observed for both samples by TM-AFM.

The presence of hedrites and spherulites in isothermally crystallized films is further substantiated by optical microscopy. The isothermally crystallized HS specimen shows the presence of giant immature spherulites, whereas the non-isothermally crystallized HS sample shows only very small birefringent features (Figure 10). That these features are due to crystallites was confirmed by the absence of any transmitted light through the crossed polarizers above the melting temperature of the sample.

The ES fraction exhibits a markedly different morphology, which reflects the very low degree of crystallinity in this sample. Lamellae are usually short, often block-like or curved, presumably due to the frequent imperfections and / or shorter isotactic sequences. More importantly, they do not show any ordered arrangements of higher hierarchical order, such as hedrites or spherulites. In addition, the cross-hatched lamellar branching typical for α-phase iPP was absent. In Figure 11, individual short lamellae in edge-on orientation can be recognized at the surface of the films. The limited length and the presence of bundling is qualitatively more pronounced in the non-isothermally crystallized samples. This indicates that the amount of crystallizable material at a certain isothermal crystallization temperature T_c may be limited, and the initially formed lamellae may serve as nucleation sites for material which crystallizes at lower temperatures. This effect, which is expected to be most important for the fraction with the lowest tendency to crystallize, i.e. the ES fraction, is thus in agreement with our observations.

We have also employed *in situ* hot stage TM-AFM[39] to determine the melting points of the lamellae seen for ES. It was found that the lamellar features disappeared at temperatures of > 100°C.[40] Despite the much lower heating rate used in the *in situ* AFM experiments compared to the DSC measurements, this temperature is significantly higher than any endotherm detected by DSC.[41]

A blend of the ES fraction and the HI fraction showed a heterogeneous morphology which was in some areas very similar to the unfractionated ePP polymer. The heterogeneity may indicate that the ES and HI components are not completely miscible. However, individual hedritic features with varying degree of perfection were observed for both isothermally and non-isothermally crystallized specimens. The presence of cross-hatching again indicates the presence of iPP in the monoclinic α-phase (Figure 12).

Discussion

Thermoplastic elastomers are an intriguing class of materials which possess the physical properties of elastomers and the processing characteristics of thermoplastics.[42] Polyolefin thermoplastic elastomers are known for both polyethylene and polypropylene.[42,43] These materials are characterized by a low degree of crystallinity, where the crystalline regions dispersed in the amorphous matrix provide physical crosslinks for the amorphous elastomeric segments of the chain.[7] The size and distribution of crystalline domains is an important determinant of the overall properties of these materials. Whereas the morphologies of for instance triblock copolymer

elastomers are determined by the thermodynamics of phase separation,[42] the morphologies of semi-crystalline polyolefin elastomers are determined by the crystallization kinetics.

In this work, we show for the first time that the crystallization of low-tacticity elastomeric polypropylenes, when crystallized either by slowly cooling from the melt or isothermally at various temperatures, yields lamellar, hedritic, and spherulitic morphologies reminiscent of much more highly crystalline polypropylenes. The beautiful fractal-like spherulitic morphology observed by TM-AFM for a 200 nm thin film of isothermally crystallized ePP for instance spans more than 60 μm (Figure 1)! A similar hedritic morphology is observed on the surface of thicker films (0.5 mm) of isothermally crystallized ePP (Figure 2). These morphologies are representative of the bulk morphology and not just surface phenomena,[22,23] which is indicated by complementary studies using polarized optical microscopy.[44] OM also revealed large birefringent hedritic and spherulitic features, which are structurally very similar to the features seen on AFM micrographs (Figures 1 vs. 4, Figures 9 vs. 10).

High-resolution TM-AFM images reveal structures most reasonably ascribed to edge-on lamellae. Evidence for these lamellae is observed even in the lowest crystallinity ES fraction (Figure 11). Several lines of evidence support our assignment of these features as lamellae. The first is the cross-hatched morphologies for several of the samples (Figure 2b). The presence of defined angles of branching of 80° is, to within the error of the experiment, equal to the expected value for cross-hatching for lamellae derived from the α-phase of isotactic PP. The size of these features (approx. 20 – 28 nm) is also consistent with those expected for polypropylene lamellae

(vide supra). Finally, the similarity of the morphologies observed in these samples to the spherulitic morphologies of other semi-crystalline polymers,[14,15,21,29,31,45] supports our assignment of these features to lamellae. The branching and splaying,[29] of chain-folded lamellar crystals leads to spherulitic morphologies in other semi-crystalline polymers. We may assume that the same mechanisms and processes occur in the ePP materials. We occasionally observed flat polygonal to round objects in ES samples, which we tentatively interpret as flat-on lamellae (Figure 13).[46,47] The observation that the majority of the lamellae are in an edge-on orientation is consistent with reports that lamellae in polyolefins, and PP in particular, grow preferentially in edge-on orientation in thin films.[14,15,32,33]

The compositional heterogeneity of the elastomeric polypropylenes derived from 2-arylindenes has allowed us to investigate the morphologies of low-crystallinity polypropylenes as a function of tacticity and crystallinity. The molecular mass of the whole sample as well as the ES and HS fractions are similar (M_n from 87,000 – 95,000) while that of the HI fraction is higher at M_n = 172,000. The tacticities of these samples, as measured by the percentage of isotactic pentads [mmmm] ranges from 21% for the ES fraction to 76% for the HI fraction. Investigation of these samples by TM-AFM has provided clear evidence for crystallinity in all fractions, including the lowest tacticity ES fraction. That the ES fraction possesses partial crystallinity is evident from the structures observed in the AFM images in Figure 11 and the fact that these structures disappear as the sample is heated above 100°C. Evidence for crystallinity in this sample was not conclusive from DSC or X-ray and estimated to be below 2% (Table 2), but at these very low levels of crystallinity, neither of these techniques can provide unambiguous evidence for crystallinity.

Investigations of both ePP and its fractions have revealed several trends: the morphologies of these samples depend both on the tacticity of the samples as well as the thermal history. For ePP as well as the HI and HS fraction, isothermal crystallization at elevated temperatures (120°C – 130°C) yields large spherulitic or hedritic morphologies reminiscent of much more highly isotactic polypropylenes. These structures are less evident in samples that were cooled slowly (approx. 5°C / min) from the melt (compare Figures 2 and 3b, Figures 4a vs. 4b, Figures 10a vs. 10b), indicating that crystallization kinetics play an important role in the evolution of these large hierarchical structures. Nevertheless, the high resolution TM-AFM images give clear evidence for cross-hatched lamellar structures for ePP, the HI fraction and the HS fraction , irrespective of the crystallization conditions.

The absence of crosshatching for the ES fraction indicates that the polymer chains possess a significant number of defects. These defects are most likely derived from atactic stereosequences which would be excluded from the chain folded lamellae, but will be enriched near the interface between lamellae and amorphous phase. For ES, the density of defects seems to be above a threshold which would still allow homoepitaxy[48] (i.e. the growth of daughter lamellae on mother lamellae in crystallographically defined angles resulting in cross-hatching) to occur. On the other hand, the rather high melting range of the ES lamellae determined by *in situ* hot stage AFM (> 100°C) suggests that the chain folded lamellae are thermally quite stable and possess a significant degree of ordering. This observation demonstrates the usefulness of AFM in analyzing phase transitions *in situ* in polymers since DSC showed no clear melting transition for the ES fraction.

The observation of lamellar morphologies for all of the samples, including the lowest crystallinity ES fraction, is indicative of long crystallizable isotactic stereosequences that can span a lamellar crystal. For ePP, these long stereosequences could be reasonably ascribed to either a mixture of isotactic polypropylene and lower tacticity polypropylenes, or to a stereoblock microstructure where the long crystallizable sequences coexist with atactic stereosequences in a given chain. The fractionation results are most consistent with a stereoblock[7,11,12] microstructure. In particular, the solubility of the ES and HS fractions implies that these fractions cannot consist of a mixture of isotactic and atactic polymer chains.[49] For the formation of lamellae, the length of the crystallizable segments or blocks must be at least of the order of a couple of fold lengths. Kravchenko et al. presented an estimate of this block length derived from the classical method of HNO_3 treatment combined with GPC [12,50] and estimated a degree of polymerization of 118 for the isotactic stereosequences for a similar sample.

The density of the cross-hatching varies systematically from ES (no cross-hatching) to ePP to HS to HI (very dense cross-hatching). This implies that the length of the stereoregular sequences increases in the same order, a trend which is fully supported by the isotacticity [mmmm] estimated from ^{13}C NMR data. The data and conclusions support strongly the notion that ePP polymers possess indeed a stereoblock structure.

Our results on the low-crystallinity polypropylenes can be compared to the elegant work of Baer and Hiltner on analogous polyethylene elastomers.[51] These authors were able to correlate the

physical properties of low-density polyethylenes with their morphologies, which were in turn correlated to the amount of comonomer, density, and crystallinity in the ethylene copolymers.[51] At high crystallinities, spherulitic morphologies were observed, at intermediate crystallinities the polyethylenes adopted a stacked lamellar morphology. For polyethylenes with densities less than 0.89 g/cm^3 a granular morphology was observed and proposed to be made up of bundled crystals or fringed micelles. The transition from lamellar morphologies to the granular "fringed micelles" coincided with the onset of elastomeric properties.

The low crystallinity polypropylenes described in this work have similar densities and mechanical properties to the polyethylenes investigated by Hiltner et al.[42] Despite the similarity in densities, degree of crystallinity, and physical properties, the morphology of the polypropylenes is markedly different. We see no evidence for “fringed-micelle” type structures at lower crystallinities, but rather observe lamellar morphologies even for the lowest crystallinity ES samples. These differences might reasonably be ascribed to the different defect distributions for the two polymers. For the polyethylenes, the defects are provided by the comonomers which, in the polymers investigated by Hiltner, are distributed randomly along the chain. As the comonomer content increases and the crystallinity of the polyethylene decreases, the average sequence length of a crystallizable ethylene sequence decreases accordingly. For the polypropylenes, the lamellar morphologies observed for the HS and ES fractions indicate that long crystallizable isotactic sequences remain even in the lowest crystallinity samples. As a consequence of this blocky microstructure, lamellar crystals can still form even when the overall percentage of crystallizable material is low.

The consequences of the morphology as described in this paper are very important to understand the mechanical behavior of these materials and to develop appropriate models that can describe this behavior. In uniaxial deformation we would expect, based on the morphological data presented here, that the ES fraction should behave very differently compared to the other fractions and the parent ePP. In uniaxial extension the lamellae of the ES can be expected to rotate into the strain direction. Assuming the chain-folding is perpendicular to the long-axis of the lamella, this would lead to chains being oriented *perpendicular* to the strain direction, whereas the other materials would show an orientation of polymer chains *parallel to* the strain direction. The latter situation is anticipated based on classical models of polymer deformation, such as the model by Peterlin.[52] Preliminary data indicate that these orientational effects do occur.[53] Thus, we may postulate that the morphology has a dramatic impact on the behavior of the material under strain and thus also on the mechanical performance. Further studies are underway to assess the changes in molecular and lamellar orientation, as well as strain-induced crystallization, during tensile flow. These results will allow us to develop a general model which describes the impact of the morphology on the corresponding materials' mechanical properties.

Conclusions

We have investigated the crystallization behavior of elastomeric polypropylene (ePP) with a density of 0.86 g/cm^3, and showed by a combination of techniques that ePP films, which were subjected to isothermal or non-isothermal temperature treatments, crystallize. We presented for the first time solid evidence that this class of materials, when crystallized isothermally from the melt, exhibits morphologies that are reminiscent of classical semi-crystalline polymers. The presence of lamellae, cross-hatching, hedrites, and spherulites was revealed by high resolution tapping mode AFM and optical microscopy. The findings reported in our present paper show that a correlation between density, melting point, and morphology observed for the low-crystallinity polyethylenes are not readily extended to ePP. These results clearly indicate that ePP possesses a block-like structure and that there is a need for a re-evaluation of the previous views on the morphology of elastomeric stereoblock polypropylene materials. Our findings have direct consequences for the interpretation of the mechanical behavior of these and very likely for other low density polyolefin elastomeric materials. Fringed micelles are not necessarily required to observe elastomeric behavior. Current work in our groups addresses the morphology of other low density polyolefins, the *in situ* study of crystallization, and the quantitative assessment of changes in molecular and lamellar orientation during tensile test experiments. This work will allow us to develop a general model which describes the impact of the thermal history on morphology and on the corresponding materials' mechanical properties.

Acknowledgment

H. S. gratefully acknowledges financial support by the Deutsche Akademischer Austauschdienst (DAAD) in the framework of the "Hochschulsonderprogramm III" and the NSF MRSEC Center on Polymer Interfaces and Macromolecular Assemblies (CPIMA) under DMR 9808677. G.G.F. and R.M.W. acknowledge support from the National Science Foundation (DMR-9910386). W.W. and J.A.P. acknowledge the support of the Stanford Synchrotron Radiation Laboratory in providing facilities used in these experiments: this work was supported by the Department of Energy Contract DE-AC03-76SF00515.

Table 1. Polymer Characterization.

Sample	%wt	M_W (10^3)[a]	PDI[a]	mmmm (%)[b]	m (%)[c]
ePP	100	201	2.3	34	73
ES	48	147	2.1	21	67
HS	42	220	2.3	44	79
HI	10	432	2.5	76	92
Blend	-	-	-	34	73

[a] Determined by high temperature GPC at BP Amoco Chemical Company.

[b] Determined by ^{13}C NMR, the fraction of five contiguous isotactic stereosequences in the polymer.

[c] Determined by ^{13}C NMR, the fraction of isotactic diades in the polymer.

Table 2. Effect of Isothermal Crystallization.

Sample	T_m (°C)[a]	ΔH_f (J/g)[a,b]	Crystallinity DSC[a] (%)	Crystallinity WAXS (%)
ePP non-isothermal	42-149	22	11	8
ePP isothermal	50-150	22	11	9
ES non-isothermal	41-45	2	1	2
ES isothermal	41-45	2	1	2
HS non-isothermal	42	32	15	11
HS isothermal	50	32	15	14
HI non-isothermal	47-155	82	39	37
HI isothermal	57-158	83	40	41
Blend non-isothermal	43-153	22	11	9
Blend isothermal	57-153	24	11	9

a Determined by DSC, endotherm scan from -20°C to 200°C at 20°C/min.

b Standard deviation of ΔH_f is ± 2 J/g.

Figure Captions

Figure 1. TM-AFM height image of ePP crystallized isothermally at 130°C in a 200 nm thin film on oxidized Si (z scale from dark to bright 200 nm).

Figure 2. TM-AFM images of ePP bulk film crystallized isothermally at 120°C (left: height image, z scale from dark to bright 3.5 μm; right: phase image).[54]

Figure 3. TM-AFM images of ePP bulk film crystallized non-isothermally (left: amplitude image, right: phase image)[54]**.**

Figure 4. Optical micrographs obtained with crossed polarizers on ePP films crystallized isothermally at 120°C (left) and non-isothermally (right).

Figure 5. Differential scanning calorimetry (DSC) endotherm scans of isothermally crystallized (120^{o}C; solid curves) and non-isothermally crystallized samples (dotted curves) of (a) ePP; (b) HS fraction; (c) HI fraction; (d) blend. Curves are shifted along y-axis for clarity.

Figure 6. Plot of WAXS intensity profiles comparing isothermally (solid curves) and non-isothermally crystallized (dotted curves) materials of (a) ePP; (b) HS fraction; (c) HI fraction; (d) blend. Crystalline peaks, as indicated for the HI fraction,[55,37] are reflection of α-phase iPP. Curves are shifted along y-axis for clarity.

Figure 7. Crystallinities normalized to the crystallinity of HI for films crystallized isothermally at 120°C as determined by various methods.[56]

Figure 8. TM-AFM images of HI bulk film crystallized isothermally at 120°C (left: amplitude image; right: phase image)[54]

Figure 9. TM-AFM images of HS bulk film crystallized isothermally at 120°C (left: amplitude image; right: phase image).[54]

Figure 10. Optical micrographs obtained with crossed polarizers on HS films crystallized isothermally at 120°C (left) and non-isothermally (right).

Figure 11. Comparison of TM-AFM phase images of isothermally (120°C; left) and non-isothermally (right) crystallized ES bulk film.[54]

Figure 12. TM-AFM images of bulk film of the blend crystallized non-isothermally (left amplitude image; right: phase image).[54]

Figure 13. TM-AFM height image (z = 7 nm) of a flat-on lamella of ES grown isothermally at 120°C for 2 hours before quenching to room temperature. Due to the slow quenching, additional PP could crystallize which gives rise to the clearly discernible rim around the lamella.

References

1 (a) Brintzinger, H. H.; Fischer, D.; Mülhaupt, R.; Rieger, B.; Waymouth, R. M. *Angew. Chem., Int. Ed. Engl.* **1995**, *34*, 1143; (b) *Metallocene-Based Polyolefins*; Scheirs, J.; Kaminsky, W., Ed.; Wiley: Chichester, 2000; Vol. 1-2.

2 (a) Ovitt, T. M.; Coates, G. W. *J. Am. Chem. Soc.* **1999**, *121*, 4072; (b) Tian, J.; Coates, G. W. *Angew*. *Chem. Int. Ed. Engl*. **2000**, *39*, 3626.

3 Deming, T. J. *Nature* **1997**, *390*, 386; (b) Deming, T. J. *J. Polym. Sci. A, Poly. Chem.* **2000**, *38*, 3011.

4 (a) Matyjaszewski, K.; Gaynor, S.; Greszta, D.; Mardare, D.; Shigemoto, T. *J. Phys. Org. Chem.* **1995**, *8*, 306; (b) Queffelec, J.; Gaynor, S. G.; Matyjaszewski, K. *Macromolecules* **2000**, *33*, 8629.

5 Benoit, D.; Chaplinski, V.; Braslau, R.; Hawker, C. J. *J. Am. Chem. Soc.* **1999**, *121*, 3904.

6 (a) Yu, S. J. M.; Conticello, V. P.; Zhang, G. H.; Kayser, C.; Fournier, M. J.; Mason, T. L.; Tirrell, D. A. *Nature* **1997**, *389*, 167; (b) Krejchi, M. T.; Atkins, E. D. T.; Waddon, A. J.; Fournier, M. J.; Mason, T. L.; Tirrell, D. A. *Science* **1994**, *265*, 1427.

7 Natta, G. *J. Polym. Sci.* **1959**, *34*, 531.

8 (a) Collette, J. W.; Ovenall, D. W.; Buck, W. H.; Ferguson, R. C. *Macromolecules* **1989**, *22*, 3858; (b) Collette, J. W.; Tullock, C. W.; MacDonald, R. N.; Buck, W. H.; Su, A. C. L.; Harrel, J. R.; Mülhaupt, R.; Anderson, B. C. *Macromolecules* **1989**, *22*, 3851; (c) Job, R. C. U.S. Patent 5,089,573, 1992; (d) Ittel, S. D. *J. Macromol. Sci. Chem.* **1990**, *A27*, 9-11.

9 (a) Mallin, D. T.; Rausch, M. D.; Lin, Y. G.; Dong, S.; Chien, J. C. W. *J. Am. Chem. Soc.* **1990**, *112*, 2030; (b) Bravakis, A. M.; Bailey, L. E.; Pigeon, M.; Collins, S. *Macromolecules* **1998**, *31*, 1000; (c) Dietrich, U.; Hackmann, M.; Rieger, B.; Klinga, M.; Leskelae, M. *J. Am. Chem. Soc.* **1999**, *121*, 4348; (d) Dreier, T.; Erker, G.; Frohlich, R.; Wibbeling, B. *Organometallics* **2000**, *19*, 4095.

10 (a) Coates, G.W.; Waymouth, R.M. *Science* **1995**, 267*, 217;* (b) Bruce, M. D.; Coates, G. W.; Hauptman, E.; Waymouth, R. M.; Ziller, J. W. *J. Am. Chem. Soc.* **1997**, *119*, 11174.

11 (a) Carlson, E. D.; Krejchi, M. T.; Shah, C. D.; Terekawa, T.; Waymouth, R. M.; Fuller, G. G. *Macromolecules* **1998**, *31*, 5343; (b) Hu, Y.; Carlson, E. D.; Waymouth, R. M.; Fuller, G. G. *Macromolecules* **1999**, *32*, 3334; (c) Kravchenko, R.; Masood, A.; Waymouth, R. M.; Myers, C. L. *J. Am. Chem. Soc.* **1998**, *120*, 2039; (d) Carlson, E. D.; Fuller, G. G.; Waymouth, R. M. *Macromolecules* **1999**, *32*, 8094; (e) Hu, Y. R.; Carlson, E. D.; Fuller, G. G.; Waymouth, R. M. *Macromolecules* **1999**, *32*, 3334.

12 Kravchenko, R. L.; Sauer, B. B.; McLean, R. S.; Keating, M. Y.; Cotts, P. M.; Kim, Y. H. *Macromolecules* **2000**, *33*, 11.

13 Numerous polymorphic forms of iPP are known: Natta, G.; Corradini, P.; Cesari, M. *Rend. Atti Acc. Naz. Lincei* **1956**, *21*, 365; (b) Keith, H. D.; Padden jr., F. J. et al. *J. Appl. Phys.* **1959**, *30*, 1485; (c) Turner-Jones, A. et al. *Makromol. Chem*. **1964**, *75*, 134; (d) Bruckner, S.; Meille, S. V.; Petraccone, V.; Pirozzi, B. *Prog. Polym. Sci*. **1991**, *16*, 361; *(e)* Auriemma, F.; deBallesteros, O. R.; DeRosa, C.; Corradini, P. *Macromolecules* **2000**, *33*, 8764 and cited references.

14 For a morphological study by AFM on α-iPP see: Schönherr, H.; Snétivy, D.; Vancso, G. J. *Polymer Bulletin* **1993**, *3*0, 567.

15 For morphological studies by AFM on β-iPP see: (a) Trifonova, D.; Varga, J.; Vancso, G. J. *Polymer Bulletin* **1998**, *41*, 341; (b) Trifonova-van Haeringen, D.; Varga, J.; Ehrenstein, G. W.; Vancso, G. J. *J. Polym. Sci. B, Polym. Phys.* **2000**, *38*, 672

16 High resolution AFM has revealed details of the molecular structure of the different modifications of iPP, see : (a) Lotz, B.; Wittmann, J. C.; Stocker, W.; Magonov, S. N.; Cantow, H. J. *Polymer Bulletin* **1991**, *26*, 209; (b) Stocker, W.; Magonov, S. N.; Cantow, H. J.; Wittmann, J. C.; Lotz, B. *Macromolecules* **1993**, *26*, 5915; (c) Snétivy, D.; Guillet, J. E.; Vancso, G. J. *Polymer* **1993**, *34*, 429; (d) Snétivy, D.; Vancso, G. J. *Polymer* **1994**, *35*, 461; (e) Stocker, W.; Graff, S.; Lang, J.; Wittmann, J. C.; Lotz, B. *Macromolecules* **1994**, *27*, 6677; (f) Stocker, W.; Magonov, S. N.; Cantow, H. J.; Wittmann, J. C.; Lotz, B. *Macromolecules* **1994**, *27*, 6690; (g) Stocker, W.; Schuhmacher, M.; Graff, S.; Thierry, A.; Wittmann, J. C.; Lotz, B. *Macromolecules* **1998**, *31*, 807.

17 Vancso, G. J in *Polypropylene: An A - Z Reference*, Karger-Kocsis, J. (Ed.), Kluwer Academic, Dordrecht, 1999, 510.

18 Waymouth, R.M.; Chen. Z.R. et. al *manuscript in preparation*.

19 Quenching with liquid nitrogen prevents further crystallization of the remaining melt as was checked by TM-AFM in independent experiments.

20 The crystallization behavior of (ultra)thin films of ePP will be reported in a separate paper: Schönherr, H.; Waymouth, R. M.; Frank, C. W. et al. *manuscript in preparation*.

21 For reviews of AFM studies on polymers, see: (a) Goh, M. C. in *Advances in Chemical Physic*s; Vol. XCI; Prigogine, I.; Rice, S. A. (Eds.); Wiley & Sons, New York, 1995; (b) Miles, M. J. in *Characterization of Solid Polymer*s; Spells, S. J. (Ed.); Chapter 2; Chapman & Hall; New York, 1994, pp. 17-55; (c) Magonov, S. N.; Reneker, D. H. *Annu. Rev. Mater. Sci.* **1997**, *27,* 175; (d) *Scanning Probe Microscopies in Polymer*s; Ratner, B. D.; Tsukruk, V. (Eds.); *ACS Symposium Series 694,* 1998; (e) *Microstructure and Microtribology of Polymer Surfaces*; Tsukruk, V.; Wahl, K. J. (Eds.); *ACS Symposium Series 741,* 1999.

22 For a discussion of TM-AFM on elastomers see: Trifonova, D.; Schönherr, H.; van der Does, L.; Janssen, P. J. P.; Noordermeer, J. W. M.; Vancso, G. J. *Rubber Chem. Techn*. **2000**, *72*, 862 and cited references.

23 Magonov, S. N.; Elings, V.; Whangbo, M.-H. *Surf. Sci.* **1997**, *372*, L385-L391.

24 The setpoint ratio was varied between 0.4 and 0.9 with no apparent change in relative contrast, i. e. the amorphous matrix always showed a phase lag relative to the crystallites and lamellae. For a discussion of image contrast and its dependence on scanning conditions see e.g. (a) reference 23, (b) Bar, G.; Thomann, Y.; Brandsch, R.; Cantow, H.-J.; Whangbo, M.-H. *Langmuir* **1997**, *13*, 3807; (c) Bar, G.; Thomann, Y.; Whangbo, M.-H. *Langmuir* **1998**, *14,* 1219; (d) Bar, G.; Brandsch, R.; Whangbo, M.-H. *Langmuir* **1998**, *14*, 7343; (e) Pickering, J. P.; Vancso, G. J. *Polymer Bulletin* **1998**, *40*, 549.

25 Wunderlich, B. *Macromolecular Physics*; Academic Press: New York, 1976; Vol.2.

26 Hobbs, J. P.; Sung, C. S. P.; Krishnan, K.; Hill, S. *Macromolecules* **1983**, *16*, 193 and cited references.

27 Sundell, T; Fageholm, H.; Crozier, H. *Polymer* **1996**, 37, 3227.

28 (a) Keller, A. in *Growth and Perfection of Crystals,* Doremus, R. H.; Roberts, B. W.; Turnbull, D., Eds.; Wiley, New York, 1958, 499-532; (b) Norton, D. R.; Keller, A. *Polymer* **1985**, *26*, 704.

29 Bassett, D. C. *Principles of Polymer Morphology*, Cambridge University Press, Cambridge 1981; (b) Bassett, D. C. *Macrom. Symp*. **1999**, *143*, 11.

30 It should be mentioned that nucleation by a small particle seen in the center of the spherulite is essential for obtaining such specimens in films with thicknesses on the order of 200 nm. In the absence of such nuclei, individual lamellae form in a dense network-like fashion.[20]

31 Geil, P. H. *Polymer Single Crystals*; Wiley Interscience: New York, 1963; Chapter 3.

32 (a) Khoury, F. *J. Res. Natl. Bureau Std*. **1966**, *70 A*, 29; (b) Padden, F. J.; Keith, H. D. *J. Appl. Phys*. **1966**, *37*, 4013; (c) Lotz, B.; Wittmann, J. C. *J. Polym. Sci., Polym. Physics* **1986**, *24*, 1541.

33 (a) Bassett, D. C.; Olley, R. H. *Polymer* **1984**, *25*, 935; (b) Olley, R. H.; Bassett, D. C. *Polymer* **1989**, *30*, 399.

34 Based on imaging calibration standards (silicon grating GT01, Mikromasch, Tallinn, Estonia) the *radii* of the tips used in our studies were estimated to be 5 - 15 nm. A quantitative deconvolution, however, was not attempted due to the uncertainty in information / penetration depth and the geometry of the experiment, i.e. it is not *a priori* clear whether and to what extent lamellae protrude from the surface.

35 Lamellar thicknesses of 13 - 17 nm were reported for crystallization temperatures of 120°C and 130°C, see Ceres, B.V.; Schultz, J. M. *J. Appl. Polym. Sci.* **1984**, *29*, 4183.

36 We have also investigated ePP films crystallized in contact with glass and Teflon surfaces. Although we observe a replication of the substrate topography into the elastomer film, the typical observations, such as crosshatched lamellae, were made in all specimens.

37 Samuels, R. J.; Yee, R. Y. *J. Polym. Sci., Part A2* **1972**, *10*, 385.

38 Cheng, S.Z.D.; Janimak, J.J.; Zhang, A.Q.; Hsieh, E.T. *Polymer* **1991**, 32, 648.

39 (a) Pearce, R.; Vancso, G. J. *Polymer* **1998**, *39*, 1237; (b) Hobbs, J. K.; McMaster, T. J.; Miles, M. J.; Barham, P. J. *Polymer* **1998**, *39*, 2437.

40 The temperature was increased in increments of ca. 5ºC. After stabilization of the imaging conditions usually two images were acquired within 8 minutes.

41 Schönherr, H.; Waymouth, R. M.; Frank, C. W. et al. *unpublished results*.

42 *Thermoplastic elastomers* Holden, G.; Legge, N. R.; Quirk, R. P.; Schroeder, H. E. (Eds.); Hanser Publishers: New York, 1996.

43 Ho, T.; Martin, J. M. in *Metallocene-Based Polyolefins*; Scheirs, J.; Kaminsky, W., Ed.; Wiley: Chichester, 2000; Vol. 2, pp 175.

44 Thin film samples (film thickness of several micrometers to millimeters) are considered representative of the bulk. In fact most of the classic morphological work on semi-crystalline polymers was and is carried out on such thin film samples by means of polarized OM.

45 Hobbs, J. K.; Miles, M. J. *Macromolecules* **2001**, *34*, 353.

46 (a) Nisman, R.; Smith, P. F.; Vancso, G. J. *Langmuir* **1994**, *10*, 1667; (b) Vancso, G. J.; Schönherr, H. in *Microstructure and Microtribology of Polymer Surfaces*; Tsukruk, V.; Wahl, K. J. (Eds.); *ACS Symposium Series 741,* 1999, Chapter 19, pp. 317 – 335.

47 Schönherr, H; Waymouth, R. M.; Hawker, C. J.; Frank, C. W. *ACS PMSE Preprints* **2001**, *84*, 453.

48 Alamo, R. G.; Brown, G. M.; Mandelkern, L.; Lehtinen, A.; Paukkeri, R. *Polymer* **1999**, *40*, 3933.

49 It has been shown by Keith and Padden that isotactic polypropylene can crystallize as minor component in a 10:90 mixture with atactic polypropylene. Keith, H. D.; Padden, F. J. *J. Appl. Phys.* **1964**, *35*, 1270.

50 Williams, T.; Blundell, D. J.; Keller, A.; Ward, I. M. *J. Polym. Sci* A-2, **1968**, *6*, 1613.

51 Bensason, S.; Minick, J.; Moet, A.; Chum, S.; Hiltner, A.; Baer, E. *J. Polym. Sci. B, Polym. Phys.* **1996**, *34*, 1301.

52 Peterlin, A. *Adv. Polym. Sci. Eng.* **1972**, 1.

53 Wiyatno, W.; Waymouth, R. M.; Gast, A. et al. *manuscript in preparation.*

54 TM-AFM amplitude and phase images are presented without absolute color scale. Since the magnitude of both signals is effected by various scan parameters, such as precise amplitude of the free vibrating cantilever, the setpoint ratio, the gains of the feedback loop etc., the values as given by the AFM software can only be considered as relative values.

55 Dean, D. M.; Rebenfeld, L.; Register, R. A.; Hsiao, B. S. *J. Mater. Sci.* **1998**, *33*, 4797.

56 The error bars correspond to the error calculated by Gauss error analysis with 2sd from multiple independent experiments as error in the individual crystallinity.

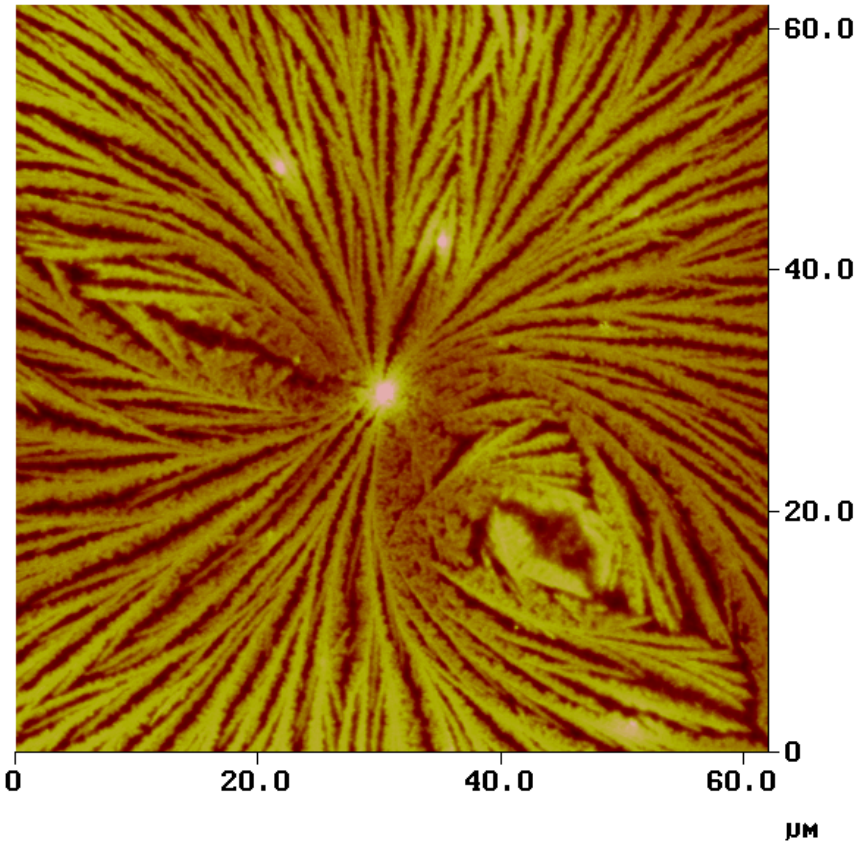

Figure 1

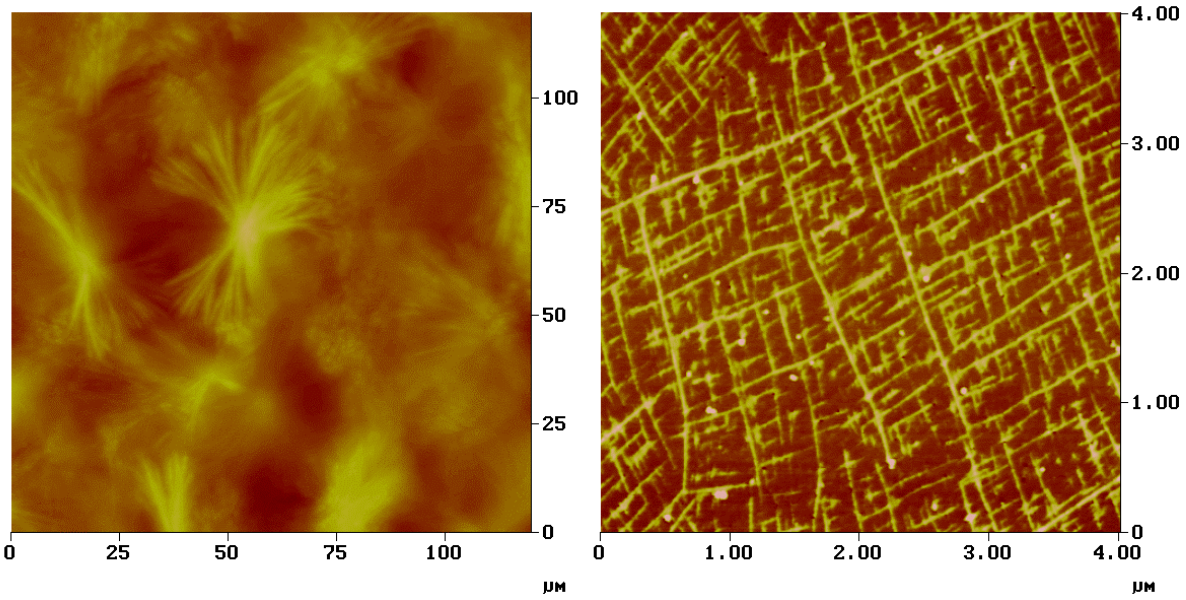
100
75
50
25
0
0
25
50
75
100
μm
4.00
3.00
2.00
1.00
0
0
1.00
2.00
3.00
4.00
μm

Figure 2

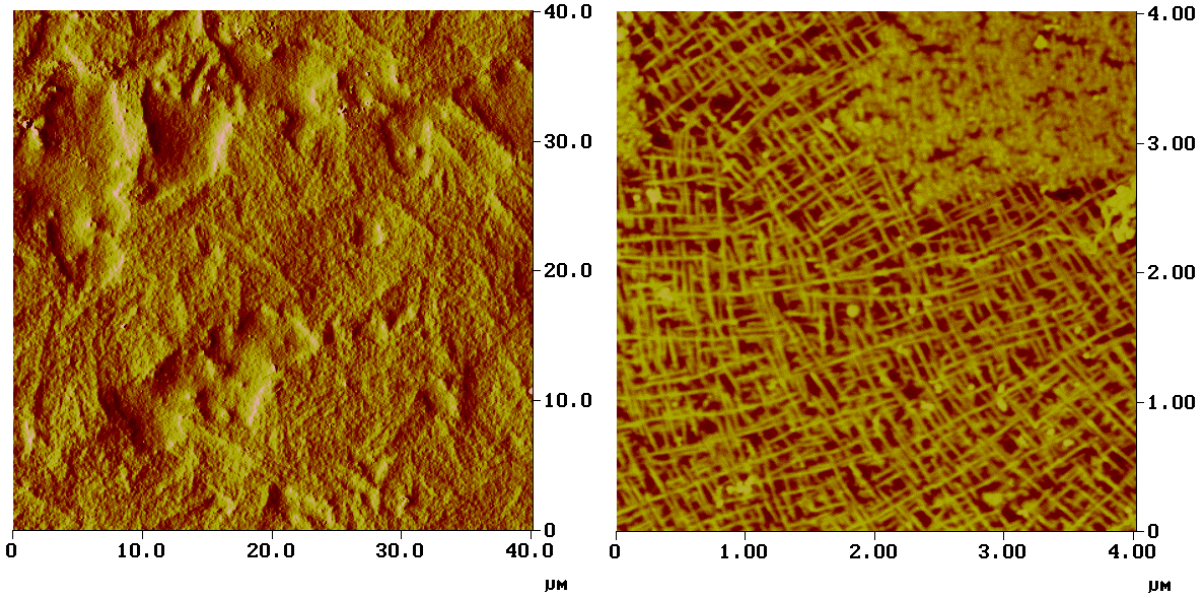
40.0
30.0
20.0
10.0
0
0
10.0
20.0
30.0
40.0
μm
4.00
3.00
2.00
1.00
0
0
1.00
2.00
3.00
4.00
μm

Figure 3

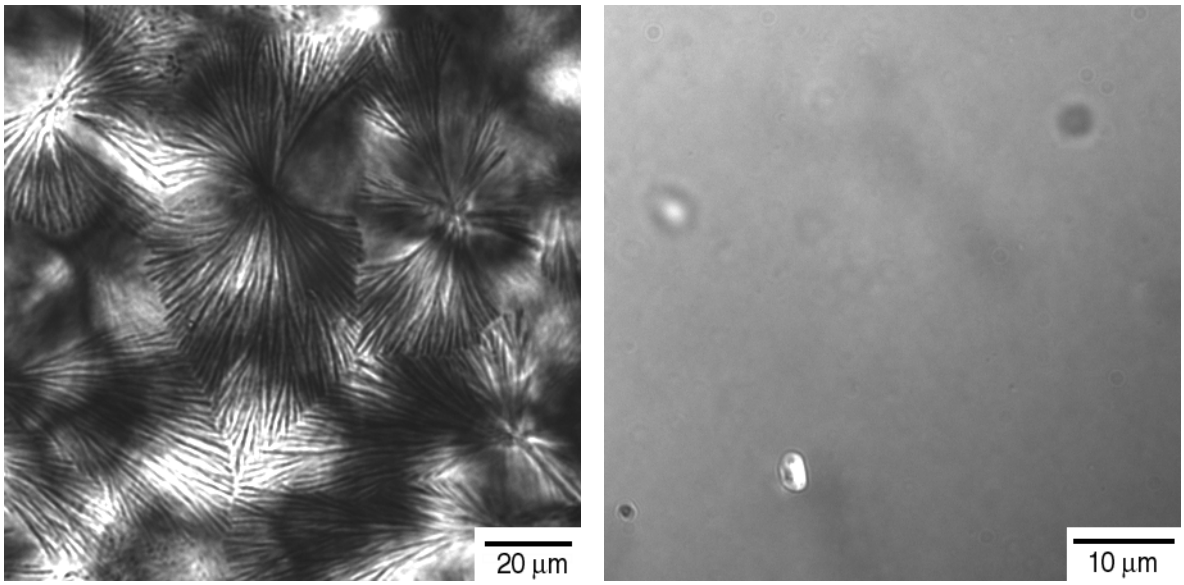

Figure 4

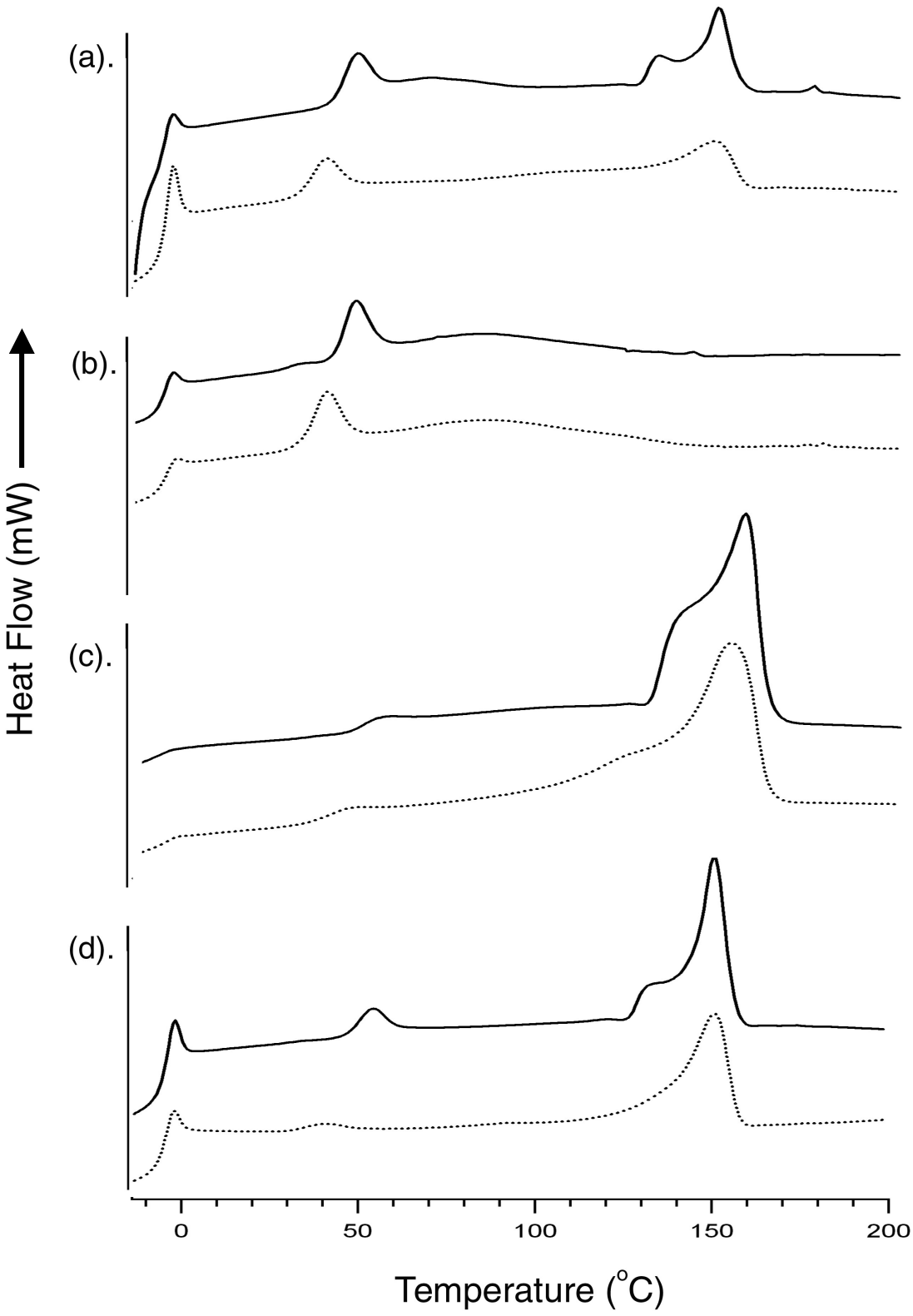

Figure 5

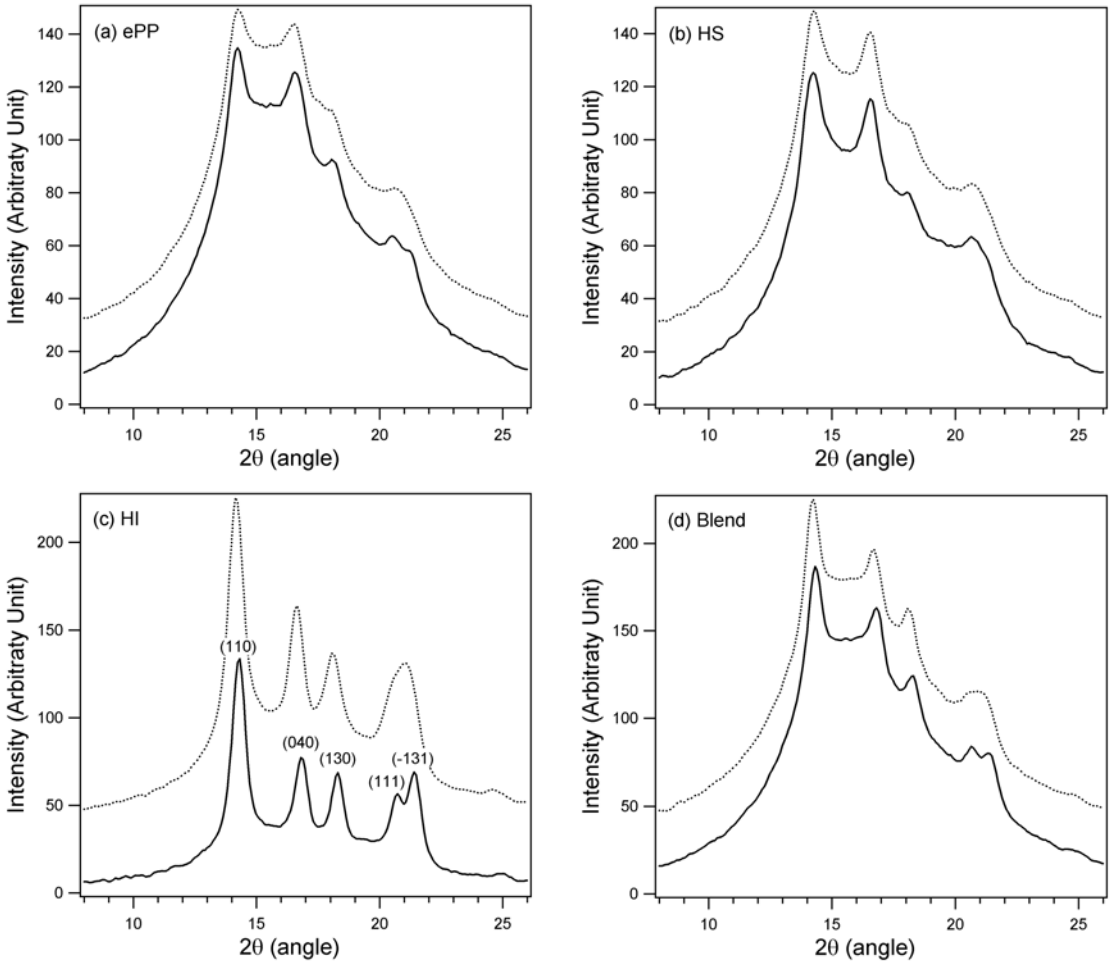
(a) ePP
(b) HS
(c) HI
(d) Blend
Intensity (Arbitraty Unit)
2θ (angle)
(110)
(040)
(130)
(111)
(-131)

Figure 6

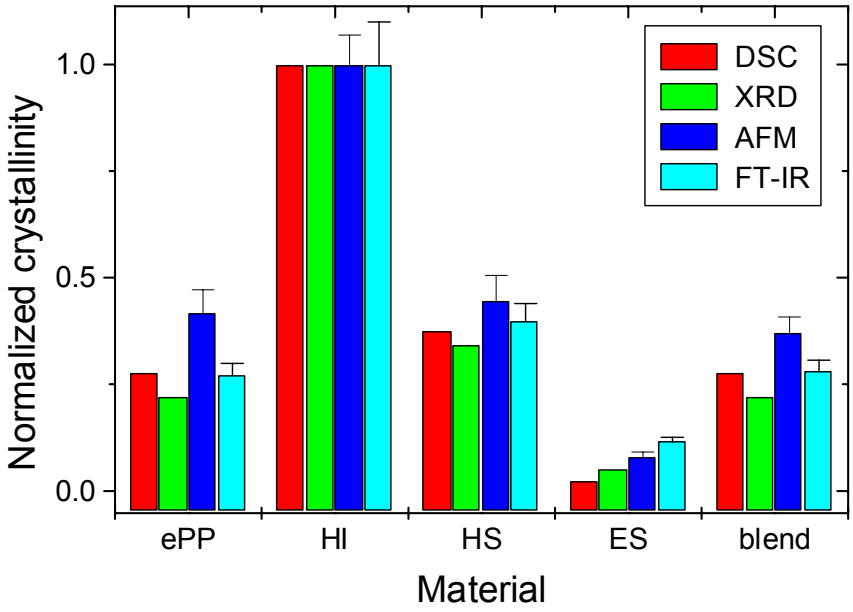
Normalized crystallinity
1.0
0.5
0.0
DSC
XRD
AFM
FT-IR
ePP
HI
HS
ES
blend
Material

Figure 7

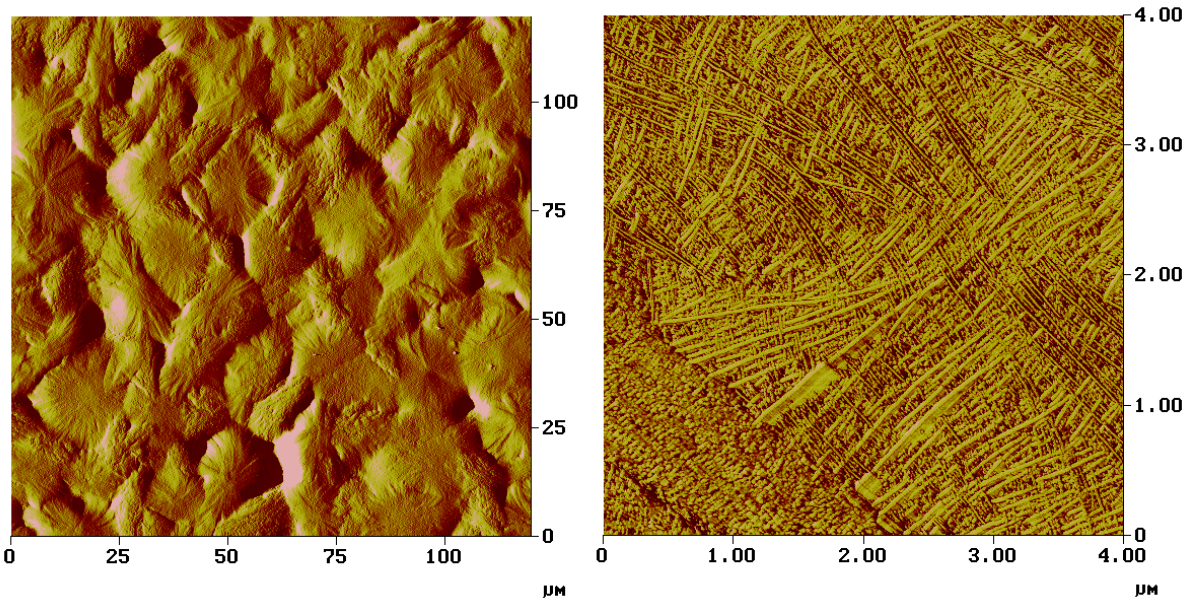
0
25
50
75
100
μm
0
25
50
75
100
0
1.00
2.00
3.00
4.00
μm
0
1.00
2.00
3.00
4.00

Figure 8

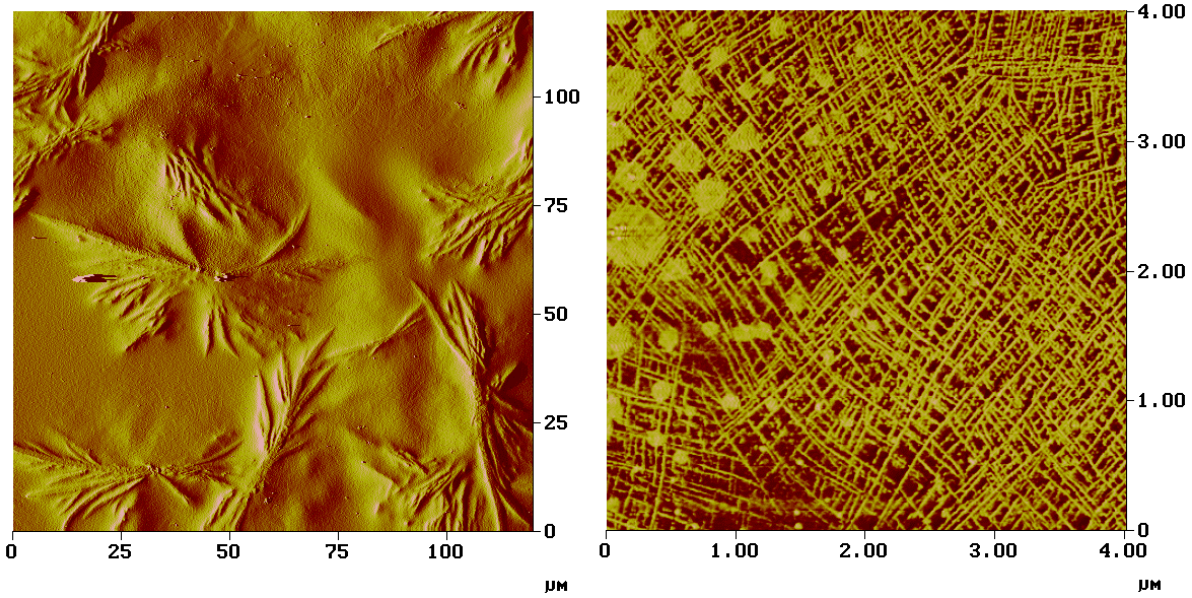
0
25
50
75
100
μm
0
25
50
75
100
0
1.00
2.00
3.00
4.00
μm
0
1.00
2.00
3.00
4.00

Figure 9

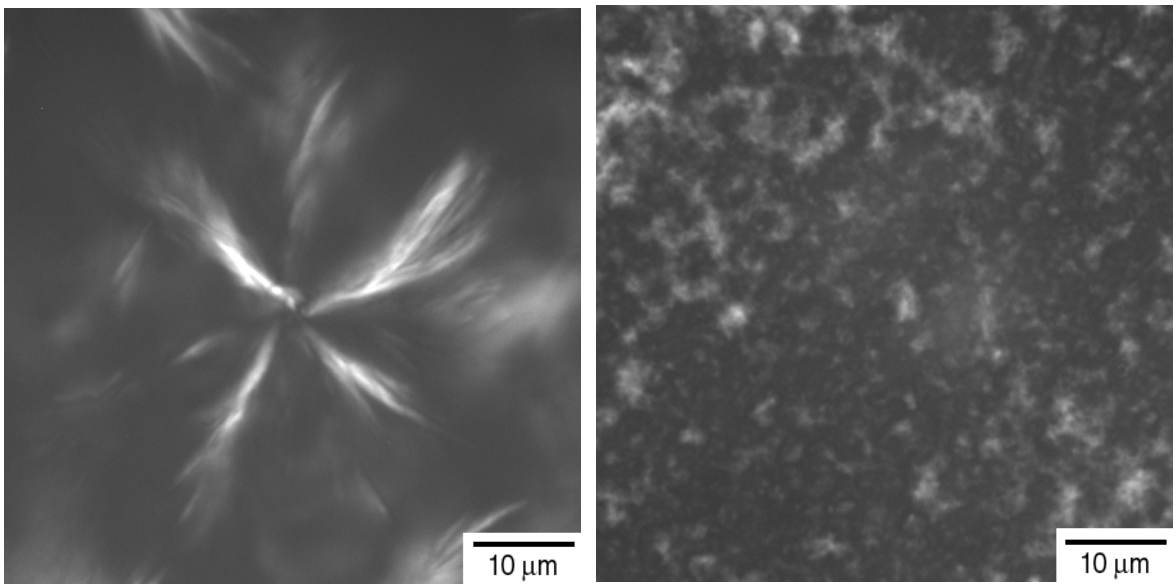

Figure 10

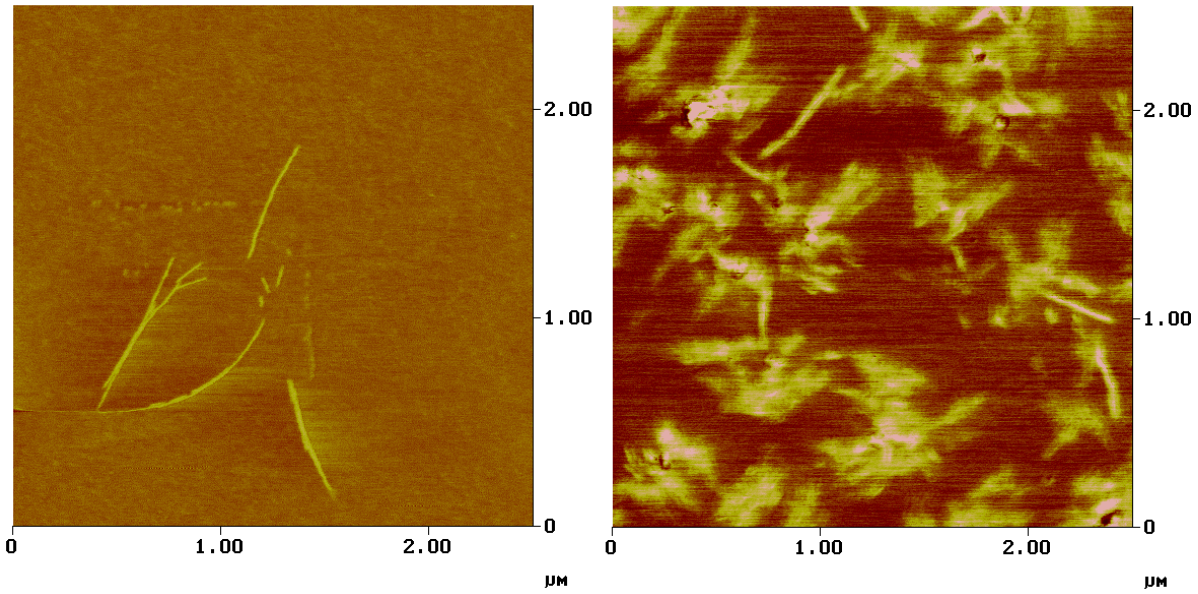

Figure 11

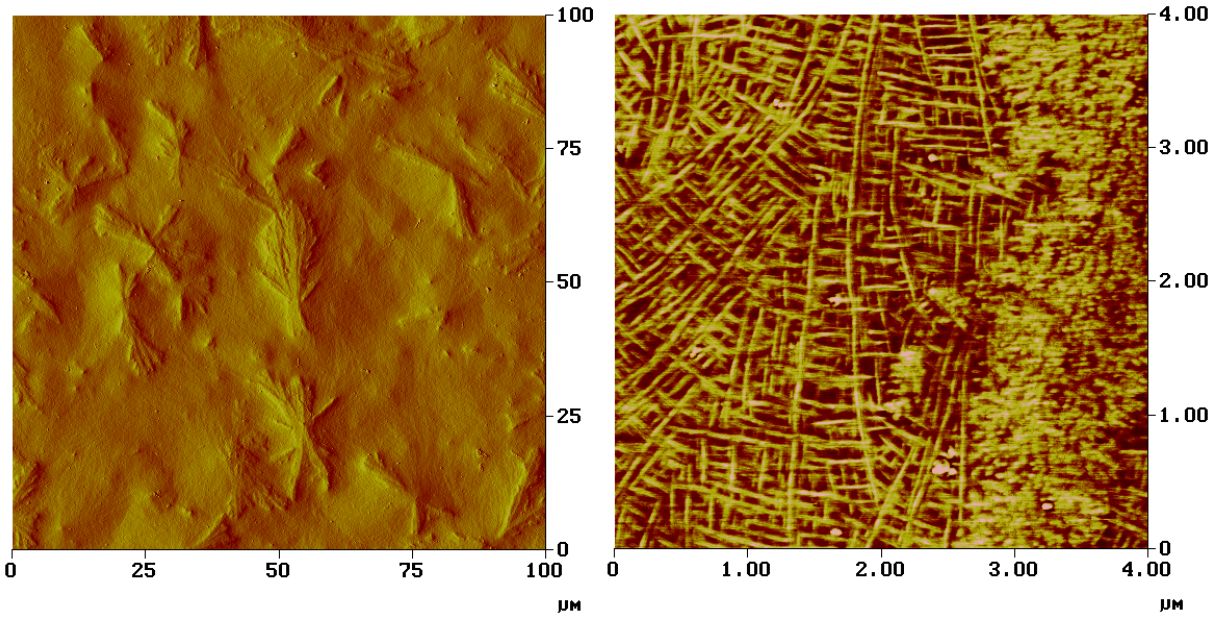
100
75
50
25
0
0
25
50
75
100
µm
4.00
3.00
2.00
1.00
0
0
1.00
2.00
3.00
4.00
µm

Figure 12

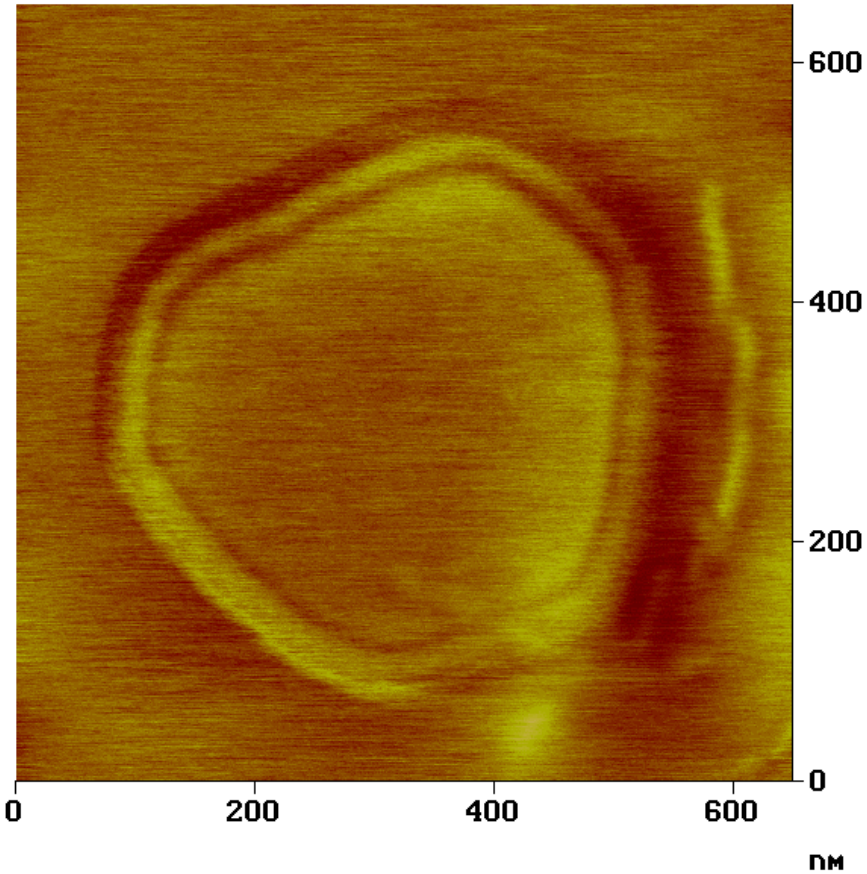

Figure 13